Distinct N and C cross-feeding networks in a synthetic mouse gut consortium

Pau Perez Escriva[1, 2], Tobias Fuhrer[1], Uwe Sauer[1, *]

[1]Institute of Molecular Systems Biology, D-BIOL, ETH Zurich, 8093 Zurich, Switzerland

[2]Systems Biology Graduate School, Zurich 8057, Switzerland

*corresponding author: sauer@ethz.ch

Abstract

The complex interactions between gut microbiome and host or pathogen colonization resistance cannot solely be understood from community composition. Missing are causal relationships such as metabolic interactions among species to better understand what shapes the microbiome. Here, we focused on metabolic niches generated and occupied by the Oligo-Mouse-Microbiota consortium, a synthetic community composed of 12 members that is increasingly used as a model for the mouse gut microbiome. Combining mono-cultures and spent medium experiments with untargeted metabolomics uncovered broad metabolic diversity in the consortium, constituting a dense cross-feeding network with more than 100 pairwise interactions. Quantitative analysis of the cross-feeding network revealed distinct C and N food webs that highlight the two Bacteroidetes consortium members *B. caecimuris* and *M. intestinale* as primary suppliers of carbon, and a more diverse group as nitrogen providers. Cross-fed metabolites were mainly carboxylic acids, amino acids, and the so far not reported nucleobases. In particular the dicarboxylic acids malate and fumarate provided a strong physiological benefit to consumers, presumably as anaerobic electron acceptors. Isotopic tracer experiments validated the fate of a subset of cross-fed metabolites, in particular the conversion of the most abundant cross-fed compound succinate to butyrate. Thus, we show that this consortium is tailored to produce the anti-inflammatory metabolite butyrate. Overall, we provide evidence for metabolic niches generated and occupied by OMM members that lays a metabolic foundation to facilitate understanding of the more complex *in vivo* behavior of this consortium in the mouse gut.

Importance

This article maps out the cross-feeding network amongst 10 members of a synthetic consortium that is increasingly used as the model mouse gut microbiota. Combining metabolomics with *in vitro* cultivations, two dense networks of carbon and nitrogen exchange are described. The vast majority of the about 100 interactions are synergistic in nature, in several cases providing distinct physiological benefits to the recipient species. These networks lay the ground work towards understanding gut community dynamics and host-gut microbe interactions.

Introduction

The mammalian gut microbiome is a complex community with thousands of bacterial species[1] that affects many facets of host physiology, ranging from metabolism and development of the immune system to protection against pathogens [2]. Extensive sequencing efforts categorized gut inhabitants and their genetic repertoire[3], but fecal microbiome composition alone does not reveal the spatial and dynamic interactions between its members and with the host. These species interactions determine succession, stability, and resilience of a community[1] and are the basis of causal relationships between microbiome composition and host physiology. Beyond correlative sequencing efforts, contemporary assessment of causal links is restricted to individual species[4] or genes[5]. Understanding more complex behavior such as pathogen colonization, however, requires considering communities at large, which is hampered by technical limitations for *in vivo* studies. Recent *in vitro* studies demonstrated that elucidating the nature of pairwise interactions between community members can be used to predict assembly and dynamic behavior a community[6,7,8]. Such pairwise interactions can be neutral, negative for both (competition) or one partner (ammensalism), or positive for both (mutualism) or one partner (commensalism). The underlying basis may be physical[9,10], quorum sensing[11], toxins, competition for nutrients[12], or metabolic cross-feeding.

To reduce the daunting complexity of natural systems, model communities of the gut microbiome with defined species composition have been used to colonize germ-free animals[13]. The primary focus of such models is to investigate complex phenotypes such as the interplay between the microbiome and host immune system or pathogen colonization resistance[14]. Recently, the Oligo-Mouse-Microbiota (OMM) consortium was introduced as a model for the mouse gut microbiome to study colonization resistance[15]. Composed of 12 natural murine isolates representing the five main gut phyla, it confers a higher colonization resistance towards the pathogen *Salmonella enterica* than the classical eight species altered Schaedler flora consortium[15]. Importantly, it is stable over time and reproducibly maintained in different animal facilities, rendering it an attractive model for the gut microbiome[16]. Although developed only recently, the OMM consortium has already helped to deepen our understanding of colonization resistance[15], inflammation[17], and development of the immune system[18].

Generally, metabolic activities and interactions between species remain largely unexplored, even for these relatively simple, synthetic consortia. Analyzing extracellular metabolic changes

upon growth in culture supernatants or in co-cultures revealed parts of a food web within the Altered Schaedler Flora consortium[19]. A first physiological characterization of microbial interactions within the OMM consortium reported primarily exploitative and interference competition during *in vitro* growth on culture supernatants[20]. From exometabolome changes in these cultures, the authors found substrate depletion profiles to correlate with growth inhibition, identified several species specific substrates and products, and singled out *Enterococcus faecalis* as the major determinant of community composition[20], although is only a low abundant member of the healthy gut microbiome[21]. Actual cross-feeding of metabolites was hypothesized between *Clostridium innocum* and *E. faecalis*. Here we focus on unraveling cross-feeding systematically between all OMM species and ask whether such metabolic interactions could also be benefitial in nature rather than the reported competitive interactions, thereby contributing to community stability. Dynamic exometabolome changes during growth in complex medium and in culture supernatants of other consortium members revealed broad metabolic diversity amongst the OMM members that gave rise to a dense cross-feeding network with more than 100 pairwise interactions, where the most abundant *in vivo* members were the main providers. We unraveled two distinct food-webs of carbon and nitrogen sources that highlight Bacteroidetes as primary suppliers of C and Firmicutes as well as the Bacteroidetes *Muribaculum intestinale* as a provider of N containing compounds. The fate of several relevant cross-fed compounds was experimentally validated with isotopic tracing, allowing us to understand their metabolic fate within the community. We thus provide evidence for key metabolic niches that are generated and occupied by members of the OMM consortium and the individual roles of each member within it.

Results

Physiologic and metabolic diversity within the OMM consortium

To characterize physiology and secretion of metabolic products, each member of the OMM consortium was grown anaerobically in brain heart infusion broth supplemented with hemin, the vitamin K precursor menadione, and mucin as the key constituent of the gut mucus (mBHI)[22]. Representing less than five percent of the fecal bacterial load of mice carrying the OMM consortium[15], the two minor constituents *Turicimonas muris* and *Acutalibacter muris* did not grow under these conditions. The other ten species achieved their maximum optical densities at 600 nm (OD) in mBHI within 25 hours (Fig. 1A). As the major constituents of the fecal community with up to 50%[21], the Bacteroidetes phylum representatives *Bacteroides caecimuris* and *M. intestinale* exhibited similar lag phases of 4-8 hours and maximum ODs, but *M. intestinale* grew substantially slower (Table 1). The Firmicutes had shorter lag phases and displayed a broader range of maximum ODs and specific growth rates (Fig. 1A, Table 1). The mucus degrading *Akkermansia muciniphila* grew only to a low maximum OD and did not grow in the absence of mucin (Table S1), suggesting that mucin is its main carbon source, as shown previously[23].

To characterize the metabolism of each species, we determined consumed and secreted metabolites by untargeted flow injection analysis time-of-flight mass spectrometry (FIA-

114 TOFMS)[24]. Specifically, three to four biological replicates were grown per species, and 8-10
115 aliquots of culture supernatants were sampled throughout the growth phase of each and
116 measured with FIA-TOFMS. 713 detected ions could be annotated to metabolites based on
117 accurate mass, assuming single deprotonation, 268 had changing time profiles in at least one of
118 the 10 investigated species (Table S2). Additionally, amino acids and short chain fatty acids were
119 quantified with a targeted liquid chromatography LC-MS method. The 29 metabolites consumed
120 by at least half of the species were primarily organic acids such as pyruvate and 2-
121 oxobutanoate, amino acid derivatives such as 4-phospho-L-aspartate, N-succinyl-L-citrulline and
122 5-hydroxy-L-tryptophan, and a few micronutrients such as ascorbate (Table S2, Fig. S1A, S1C).

123 Despite their abundance in mBHI, surprisingly none of the amino acids was consumed by the
124 majority of the members (Fig. S2). Besides serving as precursors for biomass, amino acids can
125 also be used as an energy source, for example in Stickland fermentations, where one amino acid
126 serves as an electron donor and another as an acceptor by forming carboxylic acids[25]. Many gut
127 microbes are capable of Stickland reactions that may play a role in cross-feeding in the gut[26].
128 Several OMM members have the capacity to degrade arginine, alanine, glycine, leucine, or
129 aspartate by Stickland fermentation[20]. The observed degradation of asparate by *A. muciniphila*
130 and alanine by *E. faecalisi* might thus be explained by Stickland fermentation (Fig. S2). Although
131 all OMM members could potentially degrade arginine via Stickland reduction, only four
132 members consumed it under our conditions (Fig. S2). Other types of amino acid degradation
133 were, for example, seen for lysine and histidine that were consumed by *Flavonifractor plautii*
134 and *Blautia coccoides,* respectively, the only OMM members able to degrade these amino acids
135 (Fig. S2, Table S2)[27]. Lysine degradation might be relevant *in vivo* for this consortium since its
136 degradation by *F. plautii* yields two of the three classical short chain fatty acids, acetate and
137 butyrate. Although nine species encode L-serine dehydratase orthologs that can catalyze the
138 degradation of serine to pyruvate, only the fast-growing *E. faecalis* consumed serine in larger
139 amounts and to a smaller extent *C. clostridiforme* and *F. plautii* (Fig. S2, Table S2).

140 Typical end products of fermentation such as short chain fatty acids[28] and amino acid
141 derivatives[29] were produced by some species. In particular acetate was secreted by most
142 consortium members (Fig. S2). The short chain fatty acid butyrate that is used by enterocytes as
143 an energy source[30] was produced by *C. clostridiforme, F. plautii* and *C. innocuum* (Fig. S2), where
144 the latter two have the genetic repertoire for its production from sugars[27]. Propionate was
145 secreted by *A. muciniphila* and the two Bacteroidetes members with succinate pathway genes,
146 the only propionate production pathway from carbohydrates known for this phylum[31].
147 Accumulation of amino acids, most likely from peptide digestion[32], was seen for the two
148 Bacteroidetes members and several Clostridia (Fig. S2). Amino acid fermentation products such
149 as isopropyl-malate, 4-aminobutanoate and 4-methyl-oxopentanoate and 3-methyl-2-
150 oxobutanoic acid were secreted by *C. innocuum, B. longum* and *M. intestinale* (Table S2). While
151 many metabolites were secreted by several species, not a single one was secreted by all (Fig.
152 1B). The large number of metabolites (90, 33% of all changing metabolites) secreted by only one
153 species and several taxon-specific metabolites suggests a broad metabolic diversity (Fig. S1B,

154 S1D). With 52 secreted metabolites (19% of all the metabolites detected to change over time),
155 *F. plautii* was not only the main producer in the consortium but also the unique source of 23
156 metabolites (Fig. S1D).

157 To start mapping out the metabolic interaction network from the consumption and secretion
158 patterns in monocultures, we selected for metabolites that were secreted by at least one
159 member of the consortium and consumed by one or more members. From the 268 compounds
160 with dynamic profiles, we predict 15 as one-to-many, 12 as one-to-one, 9 as many-to-one, and 5
161 as many-to-many cross-feeding interactions (Fig. 1C). In total, 41 metabolites were secreted by
162 at least one member and consumed by at least one other, hence are potentially cross-fed.

163 The OMM metabolic food web is highly connected

164 To obtain more direct evidence for cross-feeding and to capture interactions through secreted
165 metabolites that were not already present in mBHI, we performed systematic pairwise
166 cultivation experiments. For this purpose, cell-free culture supernatants of all ten species were
167 harvested at maximum OD in mBHI medium. These supernatants (i.e. spent media) were mixed
168 at a ratio of one to one with fresh mBHI, to ensure some bacterial growth, and inoculated with
169 each of the other nine species in duplicates. To assess spent media influence on consumers, we
170 compared the maximum OD obtained in the spent medium to the one obtained in undiluted
171 mBHI (Fig 2A). In one case the maximum OD of the consumer was even 10% higher than in
172 undiluted mBHI; *i.e.* when *B. caecimuris* was grown in *A. muciniphila* spent medium (Fig. 2A).
173 More generally, six out of the eight consortium members grew to nearly the same density as in
174 pure mBHI on *A. muciniphila* spent medium, suggesting that *A. muciniphila* makes breakdown
175 products of the complex glycoprotein mucin available to the community. Conversely, *A.*
176 *muciniphila* grew poorly in most spent media except those of *L. reuteri* and *B. coccoides*,
177 presumably because these two species consumed less of *A. muciniphila's* main nutrient source
178 mucin. *L. reuteri* does not have the genetic repertoire for mucin degradation while *B. coccoides*
179 does (Table S4). Hence, the latter may still degrade mucin in mBHI but provide other
180 metabolites to *A. muciniphila*. While the attained maximum ODs were generally lower than in
181 undiluted mBHI, most of them were higher than the half maximum OD that one would expect
182 from a one to one dilution (Fig. 2A), indicating consumption of additional nutrients from culture
183 supernatants or non-overlapping nutrient preferences between the two species. Besides the
184 above nutritional benefit of *A. muciniphila* culture supernatant, a particularly beneficial
185 combination was seen between *F. plautii* and *M. intestinale*. Five cultures reached lower
186 maximum ODs than expected from a one to one dilution and seven cultures did not grow at all,
187 mostly *M. intestinale*, suggesting either competition for essential nutrients or secretion of
188 inhibitory metabolites. Investigating the OMM species in pure spent media, a parallel study
189 found mainly growth inhibition[20], possibly as a consequence of nutritional competition. The high
190 frequency of positive interactions in our experiments was probably caused by mixing spent
191 medium one to one with undiluted mBHI, which avoids growth inhibition through exhaustion of
192 essential metabolites.

193 Cross-fed metabolites were identified from dynamic pattern of extracellular metabolites during
194 growth in the spent media experiments with FIA-TOF MS. Similar to fresh mBHI, 216 annotated
195 metabolites exhibited changing time profiles across all experiments. In total, 76 metabolites
196 were secreted in fresh mBHI and consumed in spent media, 31 of which were already
197 hypothesized to be cross-fed in the experiments with fresh mBHI (Fig. 1C, Table S2), providing
198 evidence for 146 metabolic cross-feeding interactions (Fig. 2B, Table S5). For example, the
199 organic acid succinate was cross-fed seven times as it was produced by several members (Table
200 S5, Fig 1C). The largest number (21) of metabolic interactions was observed for *C.*
201 *clostridioforme* when grown in the spent medium of *B. caecimuris*, although without apparent
202 effect on the maximum OD (Fig. 2A). With up to 57 consumed metabolites, *C. clostridioforme*
203 was the most promiscuous species and *M. intestinale* as the other extreme did not consume any
204 of the detected metabolites that were secreted by other consortium members (Figure 2B). The
205 small growth improvement of *F. plautii* in *M. intestinale*'s medium in the absence of detected
206 cross-feeding suggests either the presence of a not detected metabolic interaction or the
207 existence of an advantageous non-metabolic interaction. For a more systematic scoring of
208 consumers and producers, we determined the ratio of consumption versus secretion
209 interactions. Representing more than 50% of the OMM consortium in the mouse cecum and
210 colon (Fig S3)[15], the two Bacteroidetes *B. caecimuris* and *M. intestinale* had the lowest
211 consumption-secretion ratio. The second most abundant *in vivo* Firmicutes - *F. plautii* - had the
212 third lowest ratio (Table S6). Thus, *in vivo* abundant OMM members appear to have mainly a
213 provider role within the cross-feeding network through a wide range of secreted compounds.
214 The number of consumed metabolites was highly correlated with genome size (0.70), and even
215 higher when considering only cross-fed metabolites (0.80), consistent with previous
216 observations that specialist bacteria have smaller genomes than generalist bacteria[3334] (Table
217 S6).

218 The 76 cross-fed metabolites include six carboxylic acids, six amino acids or derivatives thereof,
219 seven nucleic acids, and three carbohydrates (Table S7). These metabolites may be either a
220 private or public good; *i.e.* consumed by two or more members, respectively (Fig. 2C). As typical
221 fermentation end products, carboxylic acids were significantly enriched among the public goods
222 (Fisher-exact test, p-value = 0.001). For example, the organic acid succinate was cross-fed seven
223 times. Of special interest are malate and fumarate, both secreted by *B. caecimuris* and *C.*
224 *innocuum,* that can be used as electron acceptors for respiration in anaerobic environments[35] .
225 These public goods were consumed by *L. reuteri, E. faecalis, A. muciniphila* and *C.*
226 *clostridioforme*. The presence of several consumers for electron acceptors is potentially relevant
227 for colonization resistance to *Salmonella* infections, which has been shown to require them
228 during initial gut colonization[36]. As potential nitrogen or carbon sources[29], amino acids were
229 predominant among the private goods. For example, histidine was consumed only by *B.*
230 *coccoides*, the genome of which encodes a degradation pathway that produces glutamate and
231 formate from histidine. Thus, histidine could be used by *B. coccoides* as a biomass precursor, a
232 nitrogen source, or to produce formate as an electron donor[37]. Another private good example is
233 cysteine provision by several members to *C. clostridioforme* (Table S2). Overall, we thus provide

234 evidence for a dense network of 146 cross-feeding interactions between the ten OMM
235 members (Fig. 2B), mainly through carboxylic, amino acids and nucleobases by the three
236 providers *B. caecimuris, M. intestinale*, and *F. plautii*.

237 To assess the relevance of the so far mapped interaction network and to unravel the underlying
238 metabolism, we next quantified absolute metabolite concentrations in the above spent and
239 fresh media experiments using a targeted LC-MS method covering 15 of the cross-fed
240 compounds and additional compounds that were expected to be cross-fed from the behavior in
241 fresh media (Fig. 1C). Concentrations of secreted compounds ranged from low micromolar to
242 millimolar and were generally higher for public goods. As expected, fermentation end products
243 accumulated to high concentrations with succinate being by far the most abundant cross-fed
244 metabolite, reaching 14.7 ± 0.5 mM in *B. caecimuris* spent medium. As another public good, the
245 nucleobases xanthine and hypoxanthine were secreted up to about 1 mM. Among the private
246 goods, the metabolite cross-fed at the highest concentration was histidine (~0.56 mM)(Fig. 3).

247 When calculating the C and N-mol mass balance of cross-fed metabolites from the quantified
248 consumption and production profiles, two rather distinct food webs emerge for carbon and
249 nitrogen (Fig. 3). While Bacteroidete*s* were the main provider of C compounds, with succinate
250 accounting for the major carbon flow (Fig. 3A), species from different phyla contributed to N
251 flow, including *F. plautii*, *B. longum and M. intestinale,* the latter providing the major N flow
252 through arginine (Fig. 3B). Of note, several amino acids increased over time during growth of *M.*
253 *intestinale* (Fig. S2), most likely derived from peptide digestion. Somewhat surprisingly only
254 arginine and histidine were found to be consumed by other species. Although many metabolites
255 are cross-fed (Fig. 2B), the interaction between any two members was dominated by single C-
256 and N-containing metabolites. The major mass flow of C was mediated by succinate and to a
257 lesser extent by malate and fumarate (Fig. 3A), and for N by arginine followed by the purine
258 degradation products hypoxanthine and xanthine, and histidine (Fig. 3B). Arginine catabolism
259 was previously reported for lactic acid bacteria[38] such as *L. reuteri* and *E. faecalis* via the 3 step
260 arginine deaminase system for energy generation with ornithine as a side product[38]. Both *L.*
261 *reuteri* and *E. faecalis* contain all necessary genes, including the arginine-ornithine antiporter
262 ArcD that couples arginine uptake to ornithine secretion (Table S8, S9). Consistently, we
263 observed ornithine secretion in both *L. reuteri* and *E. faecalis* in mBHI (Table S10) and that this
264 secretion was greater when grown in the spent medium of the arginine-producing *M.*
265 *intestinale*. This cross-feeding interaction might also be relevant for the host because ornithine
266 production by *Lactobacillus* has been shown to contribute to the maintenance of a healthy gut
267 mucosa[39].

268 Overall, succinate, malate and fumarate dominated cross-feeding in the C-network and the
269 amino acids arginine and histidine as well as the nucleobases xanthine and hypoxanthine the
270 cross-feeding in the N-network. In molar terms, *B. caecimuris* and *M. intestinale* were the
271 predominant providers of C and N, and *F. plautii* the predominant C consumer and at the same
272 time a relevant N provider. While microbial cross-feeding of succinate has been previously

273 reported in the gut[40], the extent to which malate and fumarate or xanthine and hypoxanthine
274 are cross-fed has not been characterized yet.

275 ## Supplementation reveals physiological benefits of cross-feeding

276 With nine compounds being cross-fed at more than 100 µM (Table S11), we next investigated
277 the physiological relevance of this C and N flux between species. Cultures of consuming species
278 were grown in mBHI medium separately supplemented with 10 mM each of the 9 compounds
279 to determine specific growth rate and maximum OD. While most supplemented metabolites did
280 not affect either of these physiological parameters, as might be expected in a rich complex
281 medium like mBHI, malate almost doubled the growth rate of *L. reuteri* and *A. muciniphila* and
282 fumarate had an even more dramatic effect on *L. reuteri* (Fig. 4A). Supplementation with N-
283 containing compounds only affected the maximum OD; i.e. a 10-20% improvement of *B.*
284 *coccoides* and *C. clostridioforme* by xanthine and the former also by histidine. Although arginine
285 has been reported as a C and N source[41], supplementation did not improve growth of *L. reuteri*
286 or *E. faecalis*. Supplementation with the amino acid cysteine had a drastic negative impact on *C.*
287 *clostridioforme* (Fig. 4A), although it was consumed during growth in spent media (Fig. 3B).

288 The higher biomass yield is most likely explained by providing energetically expensive N-
289 containing building blocks for biomass; *i.e.* synthesis of nucleotides and histidine requires
290 several ATP per molecule. The dicarboxylic acids malate and fumarate could potentially function
291 as anaerobic electron acceptors that are reduced to succinate, allowing bacteria to generate
292 more ATP[36]. To confirm their metabolic fate, we supplemented *L. reuteri* and *A. muciniphila*
293 mBHI cultures with fully ^{13}C-labelled malate. Consistent with the hypothesis, both cultures
294 consumed ^{13}C-malate and secreted fully ^{13}C-labeled succinate (Fig. 4B, Fig. S5A).

295 To assess the strong negative impact of cysteine, we supplemented *C. clostridioforme* cultures
296 with fully ^{13}C-labeled cysteine and identified pyruvate as the degradation product (Fig. S5B). The
297 inevitable byproduct of this reaction is hydrogen sulfide, an important role in maintaining
298 physiological homeostasis in the gut[42], but toxic for host and bacteria at higher
299 concentrations[43]. Indeed, increasing cysteine supplementation augmented the growth inhibition
300 (Fig. 4C), suggesting hydrogen sulfide as the inhibiting agent. This inhibition might also be
301 relevant *in vivo* because hydrogen sulfide is one of the four main gut microbiome gases[42].

302 ## Succinate cross-feeding is a main source of butyrate production in the OMM consortium

303 Since succinate accounted for the by far greatest mass flow of carbon in the OMM cross-feeding
304 network (Fig. 3A) and is a known microbiota-derived metabolite with important roles in gut
305 homeostasis, pathogen susceptibility, and inflammatory-related diseases[44], we next investigated
306 its metabolic fate. Under anaerobic conditions, succinate is generally considered as a reduced
307 end product[36] or a key intermediate of propionate synthesis by primary fermenters such as
308 Bacteroides when CO_2 is limiting[44][45]. To elucidate the fate of succinate in one of the two main
309 consumers *C. clostridioforme*, we grew cultures in mBHI supplemented with fully ^{13}C-labelled
310 succinate and analyzed its intracellular metabolome during mid exponential growth at isotopic
311 steady state by untargeted LC-MS. Among the fully labelled intracellular metabolites we found

312 several intermediates of butyrate production (Fig. S4A, Table S12). Conversion of succinate to
313 butyrate has been described for *C. kluyveri*[46] and more recently also for the gut pathogen *C.*
314 *difficile*[47]. In the latter case it was shown to constitute an important metabolic niche in the
315 absence of other succinate consumers after antibiotic treatment[47]. While this conversion to
316 butyrate does not produce ATP, it acts as an electron sink regenerating NAD+ from NADH (Fig.
317 S4B). Consistently, we observed consumption of ^{13}C-succinate and secretion of fully labelled ^{13}C-
318 butyrate (Fig. 4D), providing strong evidence for the operation of this pathway in *C.*
319 *clostridioforme*.

320 To verify whether succinate cross-feeding actually occurs in co-culture, *C. clostridioforme* and *B.*
321 *caecimuris* were grown in mono- and co-cultures. As described above (Fig. 1C; Fig. 3A),
322 monocultures of *B. caecimuris* produced succinate, but no butyrate, while *C. clostridioforme*
323 produced a small amount of butyrate (Fig. 4E). In co-culture, however, butyrate accumulated to
324 much higher levels at the expense of succinate, demonstrating succinate cross-feeding and
325 butyrate fermentation in *C. clostridioforme*. Overall these results show that the mice
326 commensal *C. clostridioforme* is a butyrate producer, and succinate cross-feeding within the
327 OMM consortium might be a relevant source of butyrate.

328 While this cross-feeding does not provide an *a priori* fitness benefit to *C. clostridioforme*,
329 butyrate is a host-relevant metabolite that can be used as a carbon source by colonocytes[48] and
330 has anti-inflammatory properties[49]. Since succinate consumption improves gut colonization of
331 the pathogen *C. difficile* in the presence of the dietary sugar sorbitol that requires NAD+ for its
332 catabolism[47], we grew *C. clostridioforme* in the rich gut microbiota medium with sorbitol or
333 succinate and sorbitol as carbon sources. Akin to *C. difficile*, succinate availability improved the
334 fitness of *C. clostridioforme*, albeit only to a small extent (Fig. S4C). Thus, we show that the
335 benefits of succinate cross-feeding for *C. clostridioforme* are context dependent, and suggest
336 that it might be a relevant interaction *in vivo* in the presence of the abundant diet-derived
337 carbon source sorbitol.

338 Discussion

339 Our results are based on an experimental approach that combines systematic *in vitro* cultivation
340 in rich and spent media with dynamic exo-metabolomics to characterize metabolic fingerprints
341 of species and infer potential metabolic interactions in microbial communities. Beyond the
342 identification of producers of well-known gut microbiome fermentation products such as
343 acetate, propionate, butyrate and lactate[40], our systematic approach mapped 152 interactions
344 in the recently introduced synthetic mouse gut consortium OMM[15]. As the major constituents
345 with up to 50% of the consortium in the mouse colon[21], the Bacteroidetes phylum
346 representatives *B. caecimuris* and *M. intestinale* were the main providers, both in terms of
347 numbers of compounds and in mass flow. The former dominated the C interaction network
348 primarily with secretion of vast amounts of succinate, but produced also the electron acceptors
349 fumarate and malate that could be used by several other species. While *M. intestinale*
350 dominated the N interaction network with the secretion of large amounts of arginine, several

351 other species contributed further N-containing compounds such as histidine and the
352 nucleobases hypoxanthine and xanthine. As the member with the largest genome, *C.*
353 *clostridioforme* was the by far most promiscuous consumer of metabolites in the consortium. *F.*
354 *plautii* assumes a special role within the community in being one of the two main consumers of
355 C in the form of succinate and a major producer of N-containing compounds.

356 While cross-feeding of carboxylic and amino acids was known to occur in the mammalian gut[50],
357 cross-feeding of nucleobases is to our knowledge a new observation. The extent of xanthine and
358 hypoxanthine interactions in our consortium and nucleobase secretion by other gut microbes
359 such as *E. coli*[51] suggests that this cross-feeding might not be limited to the OMM consortium.
360 Such purine metabolites were recently shown to affect host traits, including aging[52], irritable
361 bowel syndrome[53] or maintenance of the mucus barrier function[54]. Supplementation
362 experiments with the most abundant cross-fed metabolites demonstrated physiological benefits
363 in several cases, even in rich complex medium. Generally, N cross-feeding improved biomass
364 formation of *B. coccoides* and *C. clostridioforme*, in particular through histidine and xanthine.
365 Although cross-fed at large quantities, arginine did not provide any fitness benefit to the
366 consuming species, but led to the production of ornithine, a metabolite implied for mucosal
367 health[39] that can also induce the biosynthesis of enterobactins by *E. coli* during infection[55].

368 In contrast to the N compounds, cross-feeding with C-containing compounds affected only the
369 rate of biomass formation, presumably by allowing to produced more energy per carbon source.
370 In particular, the anaerobic electron acceptors malate and fumarate greatly increased the
371 specific growth rate of *L. reuteri* and *A. muciniphila*. In particular, the higher growth rate of *A.*
372 *muciniphila* in the presence of malate might be a relevant interaction *in vivo*, since both *A.*
373 *muciniphila* and *B. caecimuris* are the two most abundant members of the OMM consortium in
374 the cecum and colon of adult mice[21]. Alternative electron acceptors like malate and fumarate
375 have been shown to improve *in vivo* fitness of *E.coli*[35] and the pathogen *Salmonella*[56]. Their
376 production by *Bacteroides* species has been reported previously[57] and is generally linked to the
377 presence of Bacteroidetes[58].

378 While physiological benefits to the consumer are a strong argument for relevant cross-feeding,
379 a cross-feeding interaction might also be beneficial to the host. An example is succinate, that
380 was reduced by *C. clostridioforme* to butyrate, a microbiome-derived metabolite shown to
381 impact the host physiology as a carbon source, have anti-inflammatory function or act as a
382 signaling compound[47]. Butyrate production from carbohydrates or organic acids has been
383 described extensively[59], in particular conversion of succinate to butyrate by *C. kluyveri*[46] and
384 more recently also for the gut pathogen *C. difficile*[47]. Through isotopic tracing and co-culture
385 experiments with the major OMM succinate producer *B. caecimuris,* we demonstrated that also
386 *C. clostridioforme* produces butyrate from succinate, which constituted the quantitatively
387 largest cross-feeding flux in our consortium. This cross-feeding might be relevant *in vivo* not
388 only as a host source of butyrate but also for depletion of the inflammatory succinate[60]
389 produced by other species. While our findings are limited to the OMM consortium, the
390 prevalence of succinate producers such as Bacteroidetes in the gut microbiome indicates that

391 succinate cross-feeding to butyrate might be a relevant source of butyrate in the gut
392 microbiome.

393 The strongest negative fitness effect was seen for cysteine consumption by *C. clostridioforme*.
394 While cysteine inhibition of amino acid biosynthesis has been reported for *E. coli*[61], we
395 confirmed its degradation to pyruvate through isotopic tracing. This degradation releases
396 hydrogen sulfide, one of the four relevant microbiome-derived gases[42]. The origin of
397 microbiome-derived hydrogen sulfide is often associated with the presence of sulfate-reducing
398 bacteria, but members of this bacterial family are rather infrequent in the human microbiome[62]
399 and absent in the OMM consortium. Given that *C. clostridioforme* is an abundant OMM member
400 *in vivo*[21], it might play a key role in the degradation of cysteine and production of hydrogen
401 sulfide in mice harboring the OMM consortium. Consistently, a recent study reported cysteine
402 consumption in two other *C. clostridioforme* strains[58], suggesting this species as a relevant
403 cysteine consumer in the gut. Our findings are consistent with the recent notion that beyond
404 dissimilatory hydrogen sulfide formation by sulfate reducers also cysteine catabolism is
405 ubiquitous and an underestimated source of hydrogen sulfide human gut[63].

406 Comprehensive characterization of the cross-feeding network suggests that the OMM
407 consortium is highly connected at the metabolic level with distinct N and C interaction
408 networks. Quantification and metabolic characterization of the main interactions revealed
409 microbe-microbe interactions but also potential interactions with the host through metabolic
410 end-products, including butyrate, hydrogen sulfide, and ornithine. While the here used *in vitro*
411 experiments with complex mBHI and spent medium demonstrate only potential metabolic
412 interactions in the gut, the recovery of known interactions, consistency with expected *in vivo*
413 species abundance, and the demonstration of physiological relevance suggest that many of the
414 cross-feeding interactions may also be relevant *in vivo*. Our findings show that many crucial
415 metabolic features of the gut microbiota are represented within the OMM consortium and
416 strengthen its relevance as a model for the mouse gut microbiota.

417 Acknowledgement

418 We are grateful to Andrew Macpherson, Stephanie Ganal-Vonarburg and Jakob Zimmerman for
419 providing the OMM species, continuous enlightening discussions, and the former for
420 constructive feedback on the manuscript. This work was funded by the Swiss National Science
421 Foundation (SNSF Sinergia CRSII5_177164) to US.

422 Materials and Methods

423 Chemicals and strains

424 All chemicals were purchased from Sigma-Aldrich. The OMM species were kindly provided by
425 Andrew Macpherson[64].

426 ## Media preparation

427 Modified BHI (mBHI): 37 g l^{-1} Brain-Heart Infusion base, 5 mg l^{-1} hemin, 250 mg l^{-1} cysteine-HCl,
428 250 mg l^{-1} Na_2S x 9 H_2O, 0.5 mg l^{-1} menadione, and 0.25 g l^{-1} mucin from porcine stomach type II.
429 Gut microbiota medium was prepared as previously[65] except with no addition of SCFA and using
430 sorbitol (0.5% w/v) as the only carbon source.

431 ## Fresh and spent medium experiments

432 All strains were grown under anoxic conditions in an anaerobic chamber (Coy Laboratory
433 Products Inc, MI, USA) filled with an anaerobic gas mix (5% (v/v) carbon dioxide, 5% (v/v)
434 hydrogen, 90% (v/v) nitrogen) at 37°C. Overnight liquid cultures of 10 mBHI ml were prepared
435 for each species from frozen stocks. For experiments with fresh mBHI, 50 ml mBHI were
436 dispensed in 150 ml serum bottles (VWR International & Omnilab AG), sealed with a butyl
437 rubber septum and inoculated from an overnight pre-culture to an initial OD of 0.05. For every
438 consortium member, three to four replicates were incubated at 37°C and stirred at 300 rpm
439 with a small cross-shaped stir bar (2 cm diameter). Aliquots for culture density measurements
440 and metabolomics were withdrawn with a 1 ml syringe and 23G BD Precisionglide® syringe
441 needle through the rubber septum over the entire growth curve to capture lag, exponential, and
442 stationary phase (Table S13).

443 Spent media were prepared from cultures in stationary phase. For this purpose, culture broth
444 was dispended in 50 ml Falcon tubes and centrifuged at 3500 rpm for 10 minutes at 4°C, and the
445 supernatant was filter sterilized (PES membranes with 0.22 µm pore size). Aliquots of spent
446 media were stored at -20°C. Individual aliquots were thawed and equilibrated in the anaerobic
447 chamber overnight to remove dissolved oxygen before utilization. For spent media experiments,
448 Hungate tubes were filled with 10 ml of a 1:1 mixture of mBHI and spent medium from the
449 specified species. For every spent medium experiment, Hungate tubes were inoculated in
450 duplicate with 100 µl from an overnight mBHI pre-culture in stationary state to an approximate
451 initial OD of 0.05. Optical density was followed over the course of the experiment by measuring
452 it directly from the Hungate tube with a Biowave cell density meter CO8000 (VWR
453 International). Similarly, to the fresh medium experiments, samples were collected over the
454 course of the growth curve trying to capture the different phases of bacterial growth (Table
455 S13).

456 ## Mass spectrometry analysis

457 Aliquots for metabolomics analysis were prepared by centrifugation to separate cells from
458 culture supernatant and stored at -80°C until further use as previously described[66]. For
459 untargeted analysis, 40 x diluted and centrifuged samples were injected into an Agilent 6520
460 time-of flight mass spectrometer operated in negative mode at 2 Ghz EDR and with a mass /
461 charge (m/z) range of 50-1000. The mobile phase was 60:40 (v/v) isopropanol:water and 1 mM
462 NH4F at pH 9.0 for negative mode. For online mass axis correction mobile phases were
463 supplemented with hexakis(1H, 1H, 3H-tetrafluoropropoxy)phosphazine and 3-amino-1-
464 propanesulfonic acid for online mass correction. The injection sequence was randomized. Data

465 was acquired in profile mode, centroided and analyzed with Matlab (The Mathworks, Natick).
466 Missing values were filled by recursion in the raw data. Upon identification of consensus
467 centroids across all samples, ions were putatively annotated by accurate mass and isotopic
468 patterns. Starting from the a comprehensive list of bacterial metabolites database compiled by
469 extracting the metabolites present in the KEGG genomes of gut bacteria [67]. All formulas
470 matching the measured mass within a mass tolerance of 0.003 Da were enumerated. As this
471 method does not employ chromatographic separation or in-depth MS2 characterization, it is not
472 possible to distinguish between compounds with identical molecular formula. The confidence of
473 annotation reflects Level 4 but – in practice - in the case of intermediates of primary
474 metabolism it is higher because they are the most abundant metabolites in cells.

475 Short chain fatty acids were quantified with via the 3-NPH derivatization method developed by
476 Han and colleagues[68]. Briefly, 40 µl of 10-fold diluted samples were mixed with 20 µl 120 mM
477 EDC-HCL- 6% (v/v) pyridine solution and 20 µl of 200 mM 3-NPH HCL solution. Samples were
478 incubated at 37°C for 30 minutes and diluted 25 times with 10% aqueous acetonitrile. Finally,
479 samples were centrifuged 2 minutes at 3500 rpm and the clear supernatant was sued for
480 analysis. Samples were measured with the same MS system as described above.
481 Chromatographic separation was performed on a 50 x 2.1mm ,130 Å, 1.7 µm Acquity UPLC BEH
482 C18 column (Waters) using a mobile phase A: H2O, 0.1% formic acid and B: acetonitrile, 0.1%
483 formic acid. An injection volume of 2 µl was used and elution was achieved using the following
484 gradient: initial conditions, 83% A ,1100 µl/min; 0.2 min 83% A; 1.9 min 82% A; 2.8 min 60% A;
485 3.0 min 0% A; 3.50 min 0% A; 3.51 min 83% A. Online mass calibration was performed using a
486 second spray needle and a constant flow (5 ul/min) of reference solution containing purine and
487 hexakis (1H, 1H ,3H -tetrafluoropropoxy)phosphazine (HP-0921, Agilent Technologies).
488 Compounds were identified based on the retention time of chemical standards and their
489 accurate mass (tolerance 20 ppm). The MassHunter Quantitative Analysis Software (Agilent,
490 version 7.0) was used for peak integration.

491 Quantitative measurement of selected metabolites was performed with liquid chromatography
492 coupled to MS. Chromatographic separation via hydrophilic interaction (HILIC) was performed
493 on an AdvanceBio MS Spent Media column (50 x2.1mm, Agilent technologies) using a mobile
494 phase A: H_2O, 10 mM ammonium acetate, pH 9.0 and B: Acetonitrile, 10 mM ammonium
495 acetate, pH 9.0. Samples were prepared as above and diluted 5 times in 50:50 water:
496 acetonitrile. One µl of 100-fold diluted sample was injected and elution was achieved using the
497 following gradient: initial conditions, 5% A, 1000 µl/min; 0.25 min 5% A; 0.75 min 50% A; 1.0
498 min 65% A; 1.25 min 65%; 1.26 min 95%; 2.25 min 95% A. The qTOF (Agilent 6520) was
499 operated in negative mode at 2 GHz extended dynamic range and with mass/ charge (m/z)
500 range of 50-1000 and the following source parameters: VCap: 3500 C, nozzle voltage: 2000 V,
501 gas temp: 325°C m drying gas 5 l/min, nebulizer 30 psig. Online mass calibration was performed
502 using a second spray needle and a constant flow (5 ul/min) of reference solution containing
503 purine and hexakis (1H, 1H ,3H -tetrafluoropropoxy)phosphazine (HP-0921, Agilent
504 Technologies). Compounds were identified based on the retention time of chemical standards

505 and their accurate mass (tolerance 20 ppm). The MassHunter Quantitative Analysis Software
506 (Agilent, version 7.0) was used for peak integration and quantification was performed in the
507 software based on a calibration curve of chemical standards.

508 Cysteine and cystine quantification was performed with liquid chromatography coupled to MS
509 using an 5500 QTRAP triple quadrupole mass spectrometer in positive mode and MRM scan
510 type (AB SCIEX, Foster City, CA) . Separation was performed using a HILIC Plus RRHD column (1.8
511 µm, 2.1x100 mm, Agilent technologies) using a mobile phase A: H_2O with 0.1 % formic acid (v/v)
512 10 mM ammonium formate and B: Acetonitrile with 0.1% formic acid (v/v). Five µl of 80x diluted
513 sample were injected and elution was achieved using the following gradient initial conditions,
514 10% A, 400 µl/min; 2.0 min 60% A; 3.0 min 60% A; 5.0 min 10% A; 6.0 min 10% A. Data
515 acquisition was performed with Analyst 1.7.1 software (Sciex, Darmstadt, Germany) and peak
516 integration was performed using in-house software. To account for the oxidation over time of
517 cysteine in spent media[69], cysteine was quantified by adding the concentration of cysteine plus
518 two times the concentration of cystine.

519 For labelling experiments, 100-fold diluted and centrifuged samples were injected into an
520 Agilent 6546 time-of flight mass spectrometer operated in negative mode with a mass / charge
521 (m/z) range of 50-1000. Chromatographic separation was performed on a 30 x 2.1mm, 1.7 µm
522 Acquity UPLC BEH C18 column (Waters) using a mobile phase A: H2O, 0.1% acetic acid and B:
523 Methanol, 0.1% acetic acid. An injection volume of 2 µl was used and elution was achieved using
524 the following gradient: initial conditions, 83% A,1100 µl/min; 0.2 min 83% A; 1.9 min 82% A; 2.8
525 min 60% A; 3.0 min 0% A; 3.50 min 0% A; 3.51 min 83% A. Online mass calibration was
526 performed using a second spray needle and a constant flow of reference solution containing
527 purine and hexakis (1H, 1H ,3H -tetrafluoropropoxy)phosphazine (HP-0921, Agilent
528 Technologies). After processing of raw data as previously described[24], m/z features (ions) were
529 annotated by matching them to the accurate mass-to-sum formulas of a comprehensive list of
530 bacterial metabolites database with 0.001 Da mass accuracy assuming single deprotonation [M-
531 H. Notably, this metabolomics method cannot distinguish between isobaric compounds, e.g.
532 metabolites having identical m/z values (e.g. leucine vs. isoleucine).

533 ## Identification of consumed and secreted metabolites

534 Increasing and decreasing metabolites were identified from the untargeted metabolomics
535 dataset as annotated ions with significant correlation to the OD of the bacteria over time
536 (Pearson correlation coefficient >0.7, p-value<0.05) or significant goodness of linear or
537 exponential fit (R2>0.7, p-value <0.05). The latter accounts for metabolites that might be
538 exhausted before the end of the growth experiment or constantly produced throughout the
539 experiment. Furthermore, the maximum fold change between the initial time point and any
540 other point had to be higher than -1.37 for consumed metabolites and higher than 1.20 for a
541 secreted metabolite. These thresholds were determined based on an average fold change
542 observed for every annotated ion in mBHI in a dilution series. In brief, 20- to 720-fold dilutions
543 of mBHI medium were measured with FIA-MS in triplicate. Since FIA-MS is sensitive to matrix
544 effects, ion count changes cannot be directly translated into an equivalent metabolite change.

545 To remove background ions that are not derived from mBHI the above thresholds were
546 determined focusing only with annotated metabolites that had a high significant negative
547 correlation to the dilution factor (Pearson correlation < -0.75, Fig. S6A, B). To determine average
548 fold changes of consumed metabolites, we used measurements of the annotated metabolites in
549 40- 80-fold dilutions. To determine average fold changes of secreted metabolites, we used
550 measurements of annotated metabolites in 20- to 40-fold dilutions. Average fold changes were
551 1.37 and 1.20 for consumed and secreted metabolites, respectively (Fig. S6C).

552 ## *In vitro* supplementation experiments

553 Overnight liquid cultures of 5 ml of mBHI were prepared for each species from frozen stocks.
554 Solutions of supplemented metabolites were prepared in deionized water, titrated to pH 7, filter
555 sterilized (0.22 µm) and, stored at -20°C. Stock solutions of supplements were thawed and
556 equilibrated overnight in the anaerobic chamber the day before the start of the experiment.
557 Species were then grown anaerobically in in triplicates in 10 ml Hungate tubes consisting of 90%
558 (v/v) mBHI and 10% (v/v) supplement at 10 mM. Growth curves were acquired by following OD
559 with a Biowave cell density meter CO8000 (VWR International). Growth rates were inferred by
560 fitting growth-curves to OD as a function of time with a four-parameter logistic function was
561 used[70].

562 ## Isotopic tracer experiments

563 Overnight liquid cultures of 5 ml of mBHI were prepared for each species from frozen stocks.
564 Solutions of labelled supplemented metabolites were prepared in deionized water, titrated to
565 pH 7, filter sterilized (0.22 µm) and, stored at -20°C. Stock solutions of supplements were
566 thawed and equilibrated overnight in the anaerobic chamber the day before the start of the
567 experiment. Species were then grown anaerobically in triplicates in 10 ml Hungate tubes
568 consisting of 90% (v/v) mBHI and 10% (v/v) supplement at 10 mM except for ^{13}C,^{15}N-L-Cysteine
569 that was supplemented at 1 mM. Growth curves were acquired by following OD with a Biowave
570 cell density meter CO8000 (VWR International). Supernatant samples were collected and
571 processed as explained above. Intracellular samples were obtained at mid exponential phase
572 (OD of 0.4-0.6) and extracted as previously described[71]. In brief, 2 ml aliquots of cell culture
573 were filtered by vacuum filtration on a 0.45-µm filter. On the filter, cells were washed with 2 ml
574 of pre-warmed ammonium carbonate buffer at pH 7.2. Filters with cultured cells were
575 immediately transferred for extraction into 2:2:1 acetonitrile:methanol:water solution at -20°C.
576 Cells were extracted for at least 2 hours and centrifuged at 14000 g at 4°C for 20 minutes to
577 remove cell debris. Supernatants were dried at 0.12 mbar and resuspended in 100 µl of
578 deionized water.

579 ## OMM members metabolic potential assessment

580 For each of the ten cultivated strains of the OMM consortium except *L. reuteri* , *E. faecalis* and
581 *B. longum*, a list of KEGG orthologues (KO) for the protein-coding genes were obtained from the
582 KEGG genome database [72]. For *L. reuteri*, *E*. faecalis and *B. longum* the KEGG Automatic
583 Annotation Server(KAAS) with the Blast default settings[73] was used to obtain a list of KEGG

584 orthologues. Gut metabolic module (GMM) detection was performed as previously described[67].
585 In brief, GMM presence/absence was identified with a detection threshold of more than 50%
586 coverage.

587 ## Data availability

588 Raw mass spectrometry data and growth physiology data can be downloaded from
589 htttps://www.ebi.ac.uk/biostudies/, accession code S-BSST686.

590 # Bibliography

591 1. Lozupone, C. A., Stombaugh, J. I., Gordon, J. I., Jansson, J. K. & Knight, R. Diversity, stability and
592 resilience of the human gut microbiota. *Nature* **489**, 220–230 (2012).
593 2. Guarner, F. & Malagelada, J. R. Gut flora in health and disease. *Lancet* **361**, 512–519 (2003).
594 3. Turnbaugh, P. J. *et al.* The Human Microbiome Project. *Nature* **449**, 804–810 (2007).
595 4. Romano, K. A. *et al.* Metabolic, Epigenetic, and Transgenerational Effects of Gut Bacterial Choline
596 Consumption. *Cell Host Microbe* **22**, 279-290.e7 (2017).
597 5. Zimmermann, M., Zimmermann-Kogadeeva, M., Wegmann, R. & Goodman, A. L. Separating host
598 and microbiome contributions to drug pharmacokinetics and toxicity. *Science (80-.).* **363**, (2019).
599 6. Blasche, S. *et al.* Metabolic cooperation and spatiotemporal niche partitioning in a kefir microbial
600 community. *Nat. Microbiol.* **6**, 196–208 (2021).
601 7. Venturelli, O. S. *et al.* Deciphering microbial interactions in synthetic human gut microbiome
602 communities. *Mol. Syst. Biol.* **14**, (2018).
603 8. Friedman, J., Higgins, L. M. & Gore, J. Community structure follows simple assembly rules in
604 microbial microcosms. *Nat. Ecol. Evol.* **1**, 1–7 (2017).
605 9. Pande, S. *et al.* Metabolic cross-feeding via intercellular nanotubes among bacteria. *Nat.*
606 *Commun. 2015 61* **6**, 1–13 (2015).
607 10. Pal, R. R. *et al.* Pathogenic E. coli Extracts Nutrients from Infected Host Cells Utilizing Injectisome
608 Components. *Cell* **177**, 683-696.e18 (2019).
609 11. Jimenez, A. G. & Sperandio, V. Quorum Sensing and the Gut Microbiome. in *Quorum Sensing:*
610 *Molecular Mechanism and Biotechnological Application* 151–169 (Elsevier, 2019).
611 doi:10.1016/B978-0-12-814905-8.00006-X
612 12. Pickard, J. M., Zeng, M. Y., Caruso, R. & Núñez, G. Gut microbiota: Role in pathogen colonization,
613 immune responses, and inflammatory disease. *Immunological Reviews* **279**, 70–89 (2017).
614 13. Elzinga, J., van der Oost, J., de Vos, W. M. & Smidt, H. The Use of Defined Microbial Communities
615 To Model Host-Microbe Interactions in the Human Gut. *Microbiol. Mol. Biol. Rev.* **83**, (2019).
616 14. Wymore Brand, M. *et al.* The Altered Schaedler Flora: Continued Applications of a Defined Murine
617 Microbial Community. *ILAR J.* **56**, 169–178 (2015).
618 15. Brugiroux, S. *et al.* Genome-guided design of a defined mouse microbiota that confers
619 colonization resistance against Salmonella enterica serovar Typhimurium. *Nat. Microbiol.* **2**, 1–12
620 (2016).
621 16. Eberl, C. *et al.* Reproducible Colonization of Germ-Free Mice With the Oligo-Mouse-Microbiota in
622 Different Animal Facilities. *Front. Microbiol.* **10**, 2999 (2020).
623 17. Bolsega, S. *et al.* Composition of the Intestinal Microbiota Determines the Outcome of Virus-
624 Triggered Colitis in Mice. *Front. Immunol.* **10**, 1708 (2019).
625 18. Wyss, M. *et al.* Using Precisely Defined in vivo Microbiotas to Understand Microbial Regulation of
626 IgE. *Front. Immunol.* **10**, (2020).
627 19. Biggs, M. B. *et al.* Systems-level metabolism of the altered Schaedler flora, a complete gut
628 microbiota. *ISME J.* **11**, 426–438 (2017).

629 20. Weiss, A. S. *et al.* Exploring the interaction network of a synthetic gut bacterial 1 community 2 3.
630 *bioRxiv* 2021.02.25.432904 (2021). doi:10.1101/2021.02.25.432904
631 21. Bahtiyar Yilmaz, A. *et al.* Long-term evolution and short-term adaptation of microbiota strains and
632 sub-strains in mice A B Yilmaz et al ll Resource Long-term evolution and short-term adaptation of
633 microbiota strains and sub-strains in mice. *Cell Host Microbe* **29**, 1–14 (2021).
634 22. Tailford, L. E., Crost, E. H., Kavanaugh, D. & Juge, N. Mucin glycan foraging in the human gut
635 microbiome. *Front. Genet.* **6**, 81 (2015).
636 23. Derrien, M., Vaughan, E. E., Plugge, C. M. & Vos, W. M. de. Akkermansia muciniphila gen. nov., sp.
637 nov., a human intestinal mucin-degrading bacterium. *Int. J. Syst. Evol. Microbiol.* **54**, 1469–1476
638 (2004).
639 24. Fuhrer, T., Heer, D., Begemann, B. & Zamboni, N. High-Throughput, Accurate Mass Metabolome
640 Profiling of Cellular Extracts by Flow Injection–Time-of-Flight Mass Spectrometry. *Anal. Chem.* **83**,
641 7074–7080 (2011).
642 25. Neumann-Schaal, M., Jahn, D. & Schmidt-Hohagen, K. Metabolism the difficile way: The key to the
643 success of the pathogen Clostridioides difficile. *Front. Microbiol.* **10**, 219 (2019).
644 26. Medlock, G. L. *et al.* Inferring Metabolic Mechanisms of Interaction within a Defined Gut
645 Microbiota. *Cell Syst.* **7**, 245-257.e7 (2018).
646 27. Garzetti, D. *et al.* High-Quality Whole-Genome Sequences of the Oligo-Mouse-Microbiota
647 Bacterial Community. (2017). doi:10.1128/genomeA.00758-17
648 28. Morrison, D. J. & Preston, T. Formation of short chain fatty acids by the gut microbiota and their
649 impact on human metabolism. *Gut Microbes* **7**, 189–200 (2016).
650 29. Barker, H. A. *AMINO ACID DEGRADATION BY ANAEROBIC BACTERIA*. *Ann. Rev. Biochem* **50**,
651 (1981).
652 30. Litvak, Y., Byndloss, M. X. & Bäumler, A. J. Colonocyte metabolism shapes the gut microbiota.
653 *Science* **362**, eaat9076 (2018).
654 31. Reichardt, N. *et al.* Phylogenetic distribution of three pathways for propionate production within
655 the human gut microbiota. *ISME J.* **8**, 1323–1335 (2014).
656 32. Pitman, K. A., Lakshmanan, S. & Bryant, M. P. *Oligopeptide Uptake by Bacteroides ruminicola'*.
657 *JOURNAL OP BACTERIOLOGY* (1967).
658 33. Sriswasdi, S., Yang, C.-C. & Iwasaki, W. Generalist species drive microbial dispersion and
659 evolution. doi:10.1038/s41467-017-01265-1
660 34. Walter, J. & Ley, R. The Human Gut Microbiome: Ecology and Recent Evolutionary Changes.
661 (2011). doi:10.1146/annurev-micro-090110-102830
662 35. Jones, S. A. *et al.* Anaerobic Respiration of Escherichia coli in the Mouse Intestine. *Infect. Immun.*
663 **79**, 4218–4226 (2011).
664 36. Nguyen, B. D. *et al.* Import of Aspartate and Malate by DcuABC Drives H_2/Fumarate Respiration
665 to Promote *Salmonella* Gut-Luminal Colonization. *SSRN Electron. J.* (2019).
666 doi:10.2139/ssrn.3456942
667 37. Hughes, E. R. *et al.* Microbial Respiration and Formate Oxidation as Metabolic Signatures of
668 Inflammation-Associated Dysbiosis. *Cell Host Microbe* **21**, 208–219 (2017).
669 38. De Angelis, M. *et al.* Arginine catabolism by sourdough lactic acid bacteria: Purification and
670 characterization of the arginine deiminase pathway enzymes from Lactobacillus sanfranciscensis
671 CB1. *Appl. Environ. Microbiol.* **68**, 6193–6201 (2002).
672 39. Qi, H. *et al.* Lactobacillus maintains healthy gut mucosa by producing L-Ornithine. *Commun. Biol.*
673 **2**, 1–14 (2019).
674 40. Fischbach, M. A. & Sonnenburg, J. L. Eating for two: How metabolism establishes interspecies
675 interactions in the gut. *Cell Host and Microbe* **10**, 336–347 (2011).
676 41. Cunin, R., Glansdorff, N., Pierard, A. & Stalon, V. Biosynthesis and metabolism of arginine in
677 bacteria. *Microbiological Reviews* **50**, 314–352 (1986).

42. Kalantar-Zadeh, K., Berean, K. J., Burgell, R. E., Muir, J. G. & Gibson, P. R. Intestinal gases: influence on gut disorders and the role of dietary manipulations. *Nature Reviews Gastroenterology and Hepatology* **16**, 733–747 (2019).
43. Kushkevych, I., Dordević, D. & Vítězová, M. Toxicity of hydrogen sulfide toward sulfate-reducing bacteria Desulfovibrio piger Vib-7. *Arch. Microbiol.* **201**, 389–397 (2019).
44. Fernández-Veledo, S. & Vendrell, J. Gut microbiota-derived succinate: Friend or foe in human metabolic diseases? *Reviews in Endocrine and Metabolic Disorders* **20**, 439–447 (2019).
45. Caspari, D. & Macy, J. M. The role of carbon dioxide in glucose metabolism of Bacteroides fragilis. *Arch. Microbiol.* **135**, 16–24 (1983).
46. Wolff, R. A., Urben, G. W., O'Herrin, S. M. & Kenealy, W. R. Dehydrogenases involved in the conversion of succinate to 4-hydroxybutanoate by Clostridium kluyveri. *Appl. Environ. Microbiol.* **59**, (1993).
47. Ferreyra, J. A. *et al.* Gut microbiota-produced succinate promotes C. Difficile infection after antibiotic treatment or motility disturbance. *Cell Host Microbe* **16**, 770–777 (2014).
48. Donohoe, D. R. *et al.* The microbiome and butyrate regulate energy metabolism and autophagy in the mammalian colon. *Cell Metab.* **13**, 517–526 (2011).
49. Segain, J. P. *et al.* Butyrate inhibits inflammatory responses through NFκB inhibition: Implications for Crohn's disease. *Gut* **47**, 397–403 (2000).
50. Sung, J. *et al.* Global metabolic interaction network of the human gut microbiota for context-specific community-scale analysis. *Nat. Commun.* **8**, 1–12 (2017).
51. Link, H., Fuhrer, T., Gerosa, L., Zamboni, N. & Sauer, U. Real-time metabolome profiling of the metabolic switch between starvation and growth. *Nat. Methods* **12**, 1091–1097 (2015).
52. Yamauchi, T. *et al.* Gut Bacterial Species Distinctively Impact Host Purine Metabolites during Aging in Drosophila. *ISCIENCE* **23**, 101477 (2020).
53. Mars, R. A. T. *et al.* Longitudinal Multi-omics Reveals Subset-Specific Mechanisms Underlying Irritable Bowel Syndrome. *Cell* **182**, 1460-1473.e17 (2020).
54. Lee, J. S. *et al.* Microbiota-Sourced Purines Support Wound Healing and Mucous Barrier Function. *iScience* **23**, 101226 (2020).
55. Keogh, D. *et al.* Enterococcal Metabolite Cues Facilitate Interspecies Niche Modulation and Polymicrobial Infection. *Cell Host Microbe* **20**, 493–503 (2016).
56. Herp, S. *et al.* Mucispirillum schaedleri Antagonizes Salmonella Virulence to Protect Mice against Colitis. *Cell Host Microbe* **25**, 681-694.e8 (2019).
57. Chen, M. & Wolin, M. J. Influence of heme and vitamin B12 on growth and fermentations of Bacteroides species. *J. Bacteriol.* **145**, 466–471 (1981).
58. Han, S. *et al.* A metabolomics pipeline for the mechanistic interrogation of the gut microbiome. *Nat. 2021 5957867* **595**, 415–420 (2021).
59. Louis, P. & Flint, H. J. Formation of propionate and butyrate by the human colonic microbiota. *Environ. Microbiol.* **19**, 29–41 (2017).
60. Tannahill, G. M. *et al.* Succinate is an inflammatory signal that induces IL-1β through HIF-1α. *Nat. 2013 4967444* **496**, 238–242 (2013).
61. Harris, C. L. Cysteine and growth inhibition of Escherichia coli: threonine deaminase as the target enzyme. *J. Bacteriol.* **145**, 1031–1035 (1981).
62. Gibson, G. R., Macfarlane, G. T. & Cummings, J. H. Occurrence of sulphate-reducing bacteria in human faeces and the relationship of dissimilatory sulphate reduction to methanogenesis in the large gut. *J. Appl. Bacteriol.* **65**, 103–111 (1988).
63. Braccia, D. The capacity to produce hydrogen sulfide (H2S) via cysteine degradation is ubiquitous in the human gut microbiome. doi:10.1101/2021.03.24.436781
64. Macpherson, A. J. Intermicrobial and host-microbial interactions that determine the trajectory of mammalian microbial colonization in early life.

65. Goodman, A. L. *et al.* Extensive personal human gut microbiota culture collections characterized and manipulated in gnotobiotic mice. *Proc. Natl. Acad. Sci. U. S. A.* **108**, 6252–6257 (2011).
66. Paczia, N. *et al.* Extensive exometabolome analysis reveals extended overflow metabolism in various microorganisms. *Microb. Cell Fact.* **11**, 122 (2012).
67. Vieira-Silva, S. *et al.* Species-function relationships shape ecological properties of the human gut microbiome. *Nat. Microbiol.* **1**, 1–8 (2016).
68. Han, J., Lin, K., Sequeira, C. & Borchers, C. H. An isotope-labeled chemical derivatization method for the quantitation of short-chain fatty acids in human feces by liquid chromatography–tandem mass spectrometry. *Anal. Chim. Acta* **854**, 86–94 (2015).
69. Rapid Oxidation of Cysteine to Cystine in Aqueous Solutions - Implications for Spent Media Analysis | Xell AG. Available at: https://www.xell.ag/oxidation-of-cysteine-to-cystine/technical-notes/. (Accessed: 16th July 2021)
70. Paine, C. E. T. *et al.* How to fit nonlinear plant growth models and calculate growth rates: an update for ecologists. *Methods Ecol. Evol.* **3**, 245–256 (2012).
71. Buffing, M. F., Link, H., Christodoulou, D. & Sauer, U. Capacity for instantaneous catabolism of preferred and non-preferred carbon sources in Escherichia coli and Bacillus subtilis. *Sci. Reports 2018 81* **8**, 1–10 (2018).
72. Kanehisa, M. & Goto, S. KEGG: Kyoto Encyclopedia of Genes and Genomes. *Nucleic Acids Res.* **28**, 27–30 (2000).
73. Moriya, Y., Itoh, M., Okuda, S., Yoshizawa, A. C. & Kanehisa, M. KAAS: an automatic genome annotation and pathway reconstruction server. *Nucleic Acids Res.* **35**, W182–W185 (2007).

750 **Table 1. Physiological properties of the OMM members in mBHI.** Cultures were grown in 10 ml of mBHI
751 medium under anaerobic conditions in Hungate tubes.

Phyla	Species	code	max OD	μ
Firmicutes	*Flavonifractor plautii*	YL31	0.92	0.49 ± 0.08
	Blautia coccoides	YL58	1.73	0.6 ± 0.07
	Lactobacillus reuteri	I49	0.62	0.45 ± 0.04
	Clostridium innocuum	I46	1.98	1.34 ± 0.13
	Enterococcus faecalis	KB1	1.78	2.5 ± 0.01
	Acutalibacter muris	KB18	-	-
	Clostridium clostridioforme	YL32	1.74	0.54 ± 0.02
Actinobacteria	*Bifidobacterium longum*	YL2	1.01	0.91 ± 0.04
Proteobacteria	*Turicimonas muris*	YL45	-	-
Bacteroidetes	*Bacteroides caecimuris*	I48	1.18	0.47 ± 0.02
	Muribaculum intestinale	YL27	0.93	0.39 ± 0.03
Verrucomicrobia	*Akkermansia muciniphila*	YL44	0.32	0.09 ± 0.01

752
753
754
755
756
757
758
759
760
761
762
763
764
765
766
767
768
769

770 **Fig. 1. Exometabolome dynamics of OMM species in mBHI medium. A.** Growth curves of 10 OMM
771 species in mBHI medium. Shaded areas indicate the standard deviation from the mean (n=3-4 replicates).
772 **B.** Metabolic footprint heatmap of all 10 OMM species during growth in mBHI medium. Secretion is
773 indicated in red and consumption in blue. Intensities are scaled to +/- 1 by dividing each metabolite by
774 the maximum observed change in abundance in all species. Hierarchical clustering was performed for
775 metabolites, using Euclidian distances and centroid linkage. **C.** Heatmap describing the different types of
776 potential interactions extrapolated from the consumption and secretion profiles in panel B.

777 **Fig. 2. Metabolite cross-feeding among OMM members in mBHI spent medium. A.** Maximum OD of
778 OMM species during growth in a spent medium mixture of 50% culture supernatant and 50% mBHI. Data
779 points are the mean of duplicate measurements (Table S2). The species-origin of culture supernatant is
780 indicated by the color of the points. The relative maximum OD achieved by each of the other species is
781 given on the y-axis, relative to the maximum OD achieved in fresh mBHI. Relative maximum ODs of 1.1,
782 1, 0.5 and 0.4 are indicated by dotted lines. **B.** Metabolite interaction network of OMM species inferred
783 from spent medium experiments. Metabolites secreted by a producer in fresh mBHI and consumed in
784 spent media by a second species were classified as cross-fed. Consumed metabolites in spent medium
785 experiments were identified by filtering all decreasing annotated ions, either based on a significant
786 correlation with the culture OD over time (Pearson correlation coefficient<-0.7, p-value<0.05) or a
787 significant goodness of linear or exponential fit (R2>0.7, p-value<0.05). **C.** Relative metabolite class
788 distribution of public and private cross-fed compounds. Percentages were calculated from the total
789 numbers of metabolites within a class divided by the total number of metabolites, including the ones
790 without a specific class associated.

791 **Fig. 3. Carbon and nitrogen interaction networks of the OMM consortium.** Interactions were inferred
792 from growth experiments in a mix of 50% complex mBHI and 50% spent media of each OMM species. **A.**
793 Compound specific OMM carbon interaction network. **B.** Compound specific OMM nitrogen interaction
794 network. For both networks the amount of cross-fed compounds containing carbon or nitrogen was
795 quantified and multiplied by the number of carbon or nitrogen atoms per molecule, respectively. Only
796 compounds above 0.1 C-mmol or N-mmol exchange are displayed. Bacteria that represent more than
797 10% in the community are shown in larger size[21].

798 **Fig. 4. Supplementation and ^{13}C-tracing experiments reveal impact of cross-feeding interactions. A.**
799 Impact of cross-fed nutrient supplementation on maximum OD and growth rate in mBHI supplemented
800 with one metabolite of the indicated compound class (n=3 replicates per experiment). Values are shown
801 relative to the growth rate and maximum OD obtained without supplementation. Color indicates
802 metabolite class and dot size is proportional to the significance of the p-value (Student t-test). Dotted
803 horizontal lines at 1.1 and 0.9 are shown for reference. **B.** Extracellular time course of fully ^{13}C-labeled
804 succinate and malate in *L. reuteri* mBHI cultures supplemented with ^{13}C-malate. Shaded areas represent
805 the standard deviation from the experiments (n=3 replicates) **C.** Normalized area under the OD curve of
806 *C. clostridioforme* grown in mBHI supplemented with different concentrations of cysteine. Shaded areas
807 represent the standard deviation from the mean (n= 3 replicates). **D.** Levels of ^{13}C-succinate and ^{13}C-
808 butyrate over time when *C. clostridioforme* was grown in mBHI supplemented with ^{13}C-succinate. Shaded
809 areas represent the standard deviation from the mean (n = 3 replicates) **E.** Levels of succinate and
810 butyrate in mono-cultures and co-culture of *C. clostridioforme* and *B. caecimuris* in GMM normalized to
811 the maximum value across all experiments (n= 3 replicates).

812

813 **Supplementary Figure 1 A.** Metabolites consumed (blue) by more than half of the OMM members.
814 Metabolites that were not detected as abundant in fresh mBHI are shown in bold letters. Intensities are
815 scaled to +/- 1 by dividing each metabolite by the maximum observed change in abundance in all species.
816 **B.** Metabolites that were uniquely secreted by one member of the consortium. Metabolites that were
817 not detected as abundant in fresh mBHI are shown in bold letters. Alternative annotation within the
818 mass tolerance of 3 mDa are indicated where present. **C.** Upset plot of consumed metabolites by the
819 OMM species. **D.** Upset plot of produced metabolites by the OMM species.

820 **Supplementary Figure 2** Consumption (blue) and secretion (red) of relevant metabolite classes by OMM
821 species. Consumption or secretion was inferred by comparing late stationary phase concentrations in
822 spent media to fresh mBHI medium concentrations, scaled to +/- 1 by dividing the relative concentration
823 of each metabolite by the maximum observed change in abundance in all species. **A.** Nucleic acid profiles
824 determined by untargeted metabolomics analysis with FIA-MS. **B.** Short chain fatty acid profiles
825 determined by 3-NPH derivatization[68] coupled with targeted metabolomics. **C.** Vitamin and cofactor
826 profile determined by untargeted metabolomics analysis with FIA-MS. **D.** Amino acid profile determined
827 by HILIC LC-MS. Asterisk's indicate species with the ability to degrade an amino acid via Stickland
828 fermentation that consumed the respective amino acid.

829 **Supplementary Figure 3.** Relative abundance of OMM members in mice colonized with the OMM
830 consortium. Relative abundance in three different locations was determined by metagenomics
831 sequencing. Data was taken from Yilmaz *et al*[21].

832 **Supplementary Figure 4. A.** Succinate to butyrate conversion pathway proposed in *C. clostridioforme*.
833 Metabolites highlighted in bold were detected as fully labelled intracellularly when *C. clostridioforme*
834 was supplemented with ^{13}C-succinate **B.** Growth of *C. clostridioforme* in gut microbiota medium with
835 either sorbitol or sorbitol and succinate. Shaded areas represent the standard deviation from the mean
836 (n=3).

837 **Supplementary Figure 5. A.** Time course of extracellular fully ^{13}C-labeled succinate and malate in *A.*
838 *muciniphila* in mBHI cultures supplemented with ^{13}C-malate. Shaded areas represent the standard
839 deviation from the experiments (n=3). **B.** Intracellular fully labelled fraction of pyruvate in *C.*
840 *clostridioforme* when grown with ^{13}C-cysteine or with ddH_2O (n=3).

841 **Supplementary Figure 6. A.** Distribution of Pearson correlation coefficients between dilution factor and
842 ion intensity of the metabolites annotated in mBHI via FIA-MS. **B.** Normalized ion intensity over the
843 dilution factor for metabolites with a Pearson correlation coefficient below -0.75. Shaded areas
844 represent the standard deviation from the mean (n=3) **C.** Average fold change for annotated ions that
845 had a Pearson correlation coefficient below -0.75 from 20- to 40-fold dilution (increase) and from 40- to
846 80-fold dilution (decrease).

Figure 1

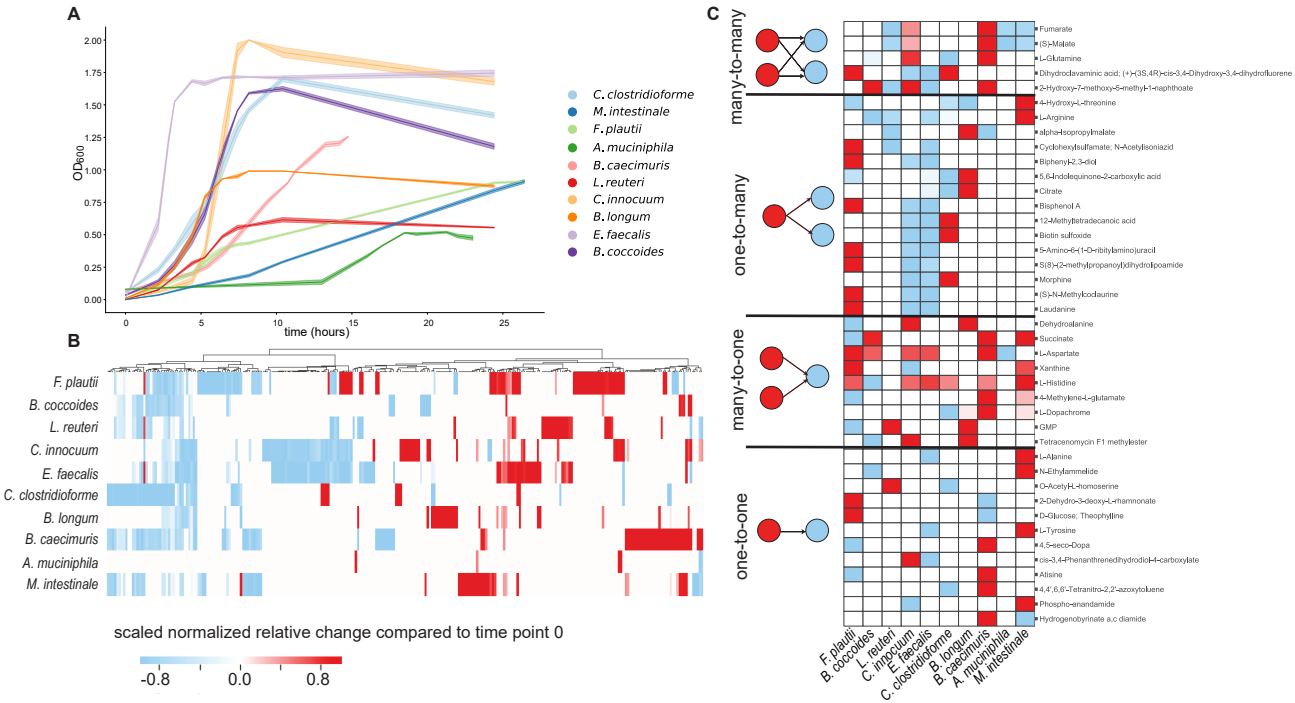
A
OD600
time (hours)
C. clostridioforme
M. intestinale
F. plautii
A. muciniphila
B. caecimuris
L. reuteri
C. innocuum
B. longum
E. faecalis
B. coccoides
B
F. plautii
B. coccoides
L. reuteri
C. innocuum
E. faecalis
C. clostridioforme
B. longum
B. caecimuris
A. muciniphila
M. intestinale
scaled normalized relative change compared to time point 0
-0.8
0.0
0.8
C
many-to-many
one-to-many
many-to-one
one-to-one
Fumarate
(S)-Malate
L-Glutamine
Dihydrocadavaminic acid; (+)-(3S,4R)-cis-3,4-Dihydroxy-3,4-dihydrofluorene
2-Hydroxy-7-methoxy-5-methyl-1-naphthoate
4-Hydroxy-L-threonine
L-Arginine
alpha-Isopropylmalate
Cyclohexylsulfamate; N-Acetylisoniazid
Biphenyl-2,3-diol
5,6-Indolequinone-2-carboxylic acid
Citrate
Bisphenol A
12-Methyltetradecanoic acid
Biotin sulfoxide
5-Amino-6-(1-D-ribitylamino)uracil
S(8)-(2-methylpropanoyl)dihydrolipoamide
Morphine
(S)-N-Methylcodaurine
Laudanine
Dehydroalanine
Succinate
L-Aspartate
Xanthine
L-Histidine
4-Methylene-L-glutamate
L-Dopachrome
GMP
Tetracenomycin F1 methylester
L-Alanine
N-Ethylammelide
O-Acetyl-L-homoserine
2-Dehydro-3-deoxy-L-rhamnonate
D-Glucose; Theophylline
L-Tyrosine
4,5-seco-Dopa
cis-3,4-Phenanthrenedihydrodiol-H-carboxylate
Atisine
4,4',6,6'-Tetranitro-2,2'-azoxytoluene
Phospho-anandamide
Hydrogenobyrinate a,c diamide
F. plautii
B. coccoides
L. reuteri
C. innocuum
E. faecalis
C. clostridioforme
B. longum
B. caecimuris
A. muciniphila
M. intestinale

Figure 2

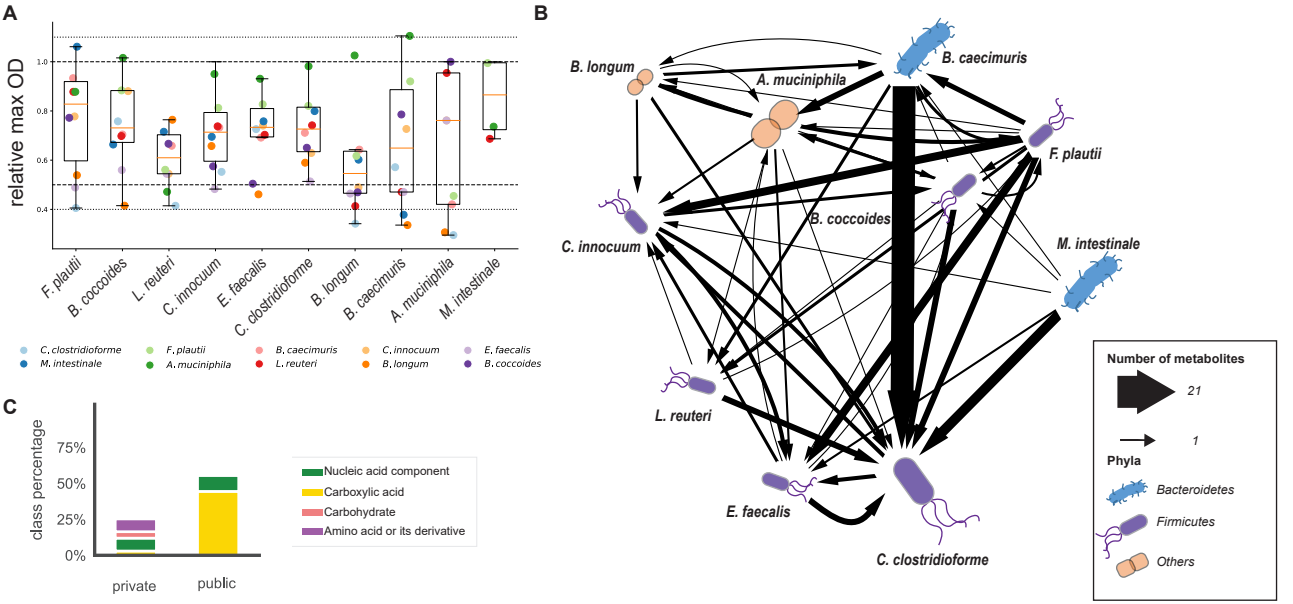
A
relative max OD
1.0
0.8
0.6
0.4
F. plautii
B. coccoides
L. reuteri
C. innocuum
E. faecalis
C. clostridioforme
B. longum
B. caecimuris
A. muciniphila
M. intestinale
C. clostridioforme
M. intestinale
F. plautii
A. muciniphila
B. caecimuris
L. reuteri
C. innocuum
B. longum
E. faecalis
B. coccoides
B
B. longum
A. muciniphila
B. caecimuris
F. plautii
B. coccoides
C. innocuum
M. intestinale
L. reuteri
E. faecalis
C. clostridioforme
Number of metabolites
21
1
Phyla
Bacteroidetes
Firmicutes
Others
C
class percentage
75%
50%
25%
0%
private
public
Nucleic acid component
Carboxylic acid
Carbohydrate
Amino acid or its derivative

Figure 3

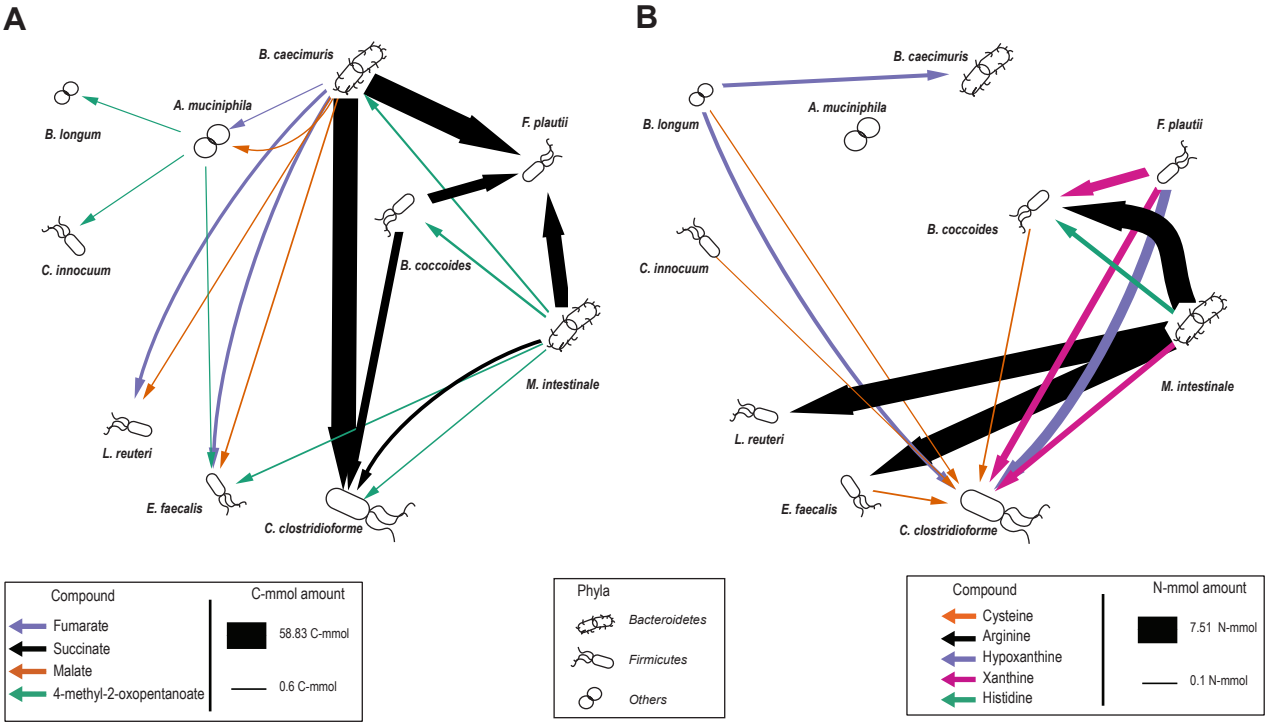
A
B. caecimuris
A. muciniphila
B. longum
F. plautii
C. innocuum
B. coccoides
M. intestinale
L. reuteri
E. faecalis
C. clostridioforme
B
B. caecimuris
B. longum
A. muciniphila
F. plautii
B. coccoides
C. innocuum
M. intestinale
L. reuteri
E. faecalis
C. clostridioforme
Compound
Fumarate
Succinate
Malate
4-methyl-2-oxopentanoate
C-mmol amount
58.83 C-mmol
0.6 C-mmol
Phyla
Bacteroidetes
Firmicutes
Others
Compound
Cysteine
Arginine
Hypoxanthine
Xanthine
Histidine
N-mmol amount
7.51 N-mmol
0.1 N-mmol

Figure 4

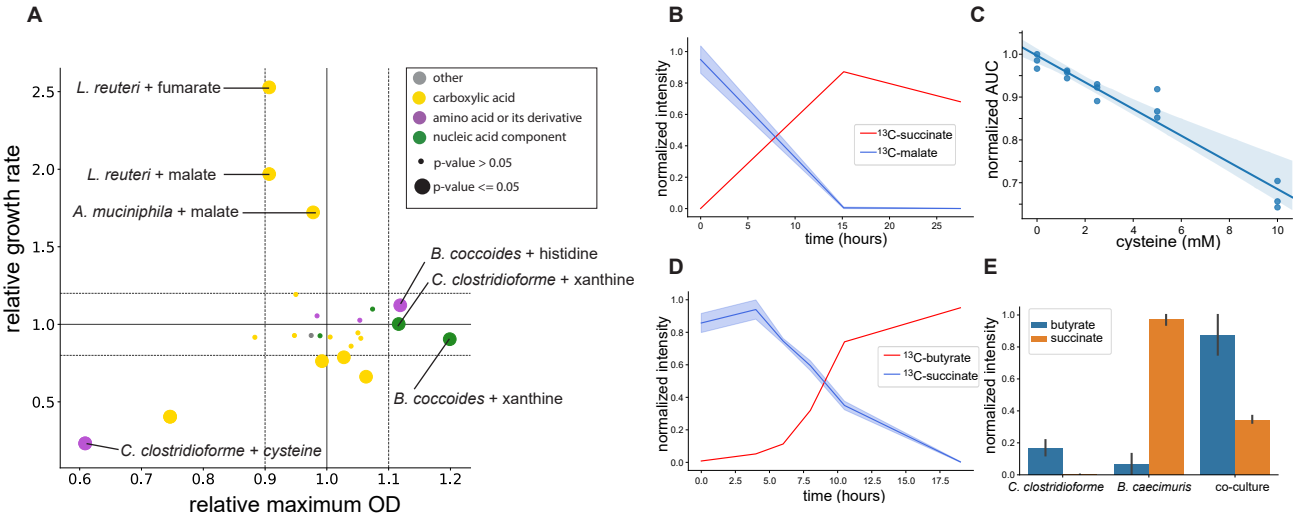
A
relative growth rate
relative maximum OD
L. reuteri + fumarate
L. reuteri + malate
A. muciniphila + malate
B. coccoides + histidine
C. clostridioforme + xanthine
B. coccoides + xanthine
C. clostridioforme + cysteine
other
carboxylic acid
amino acid or its derivative
nucleic acid component
p-value > 0.05
p-value <= 0.05
B
normalized intensity
time (hours)
13C-succinate
13C-malate
C
normalized AUC
cysteine (mM)
D
normalized intensity
time (hours)
13C-butyrate
13C-succinate
E
normalized intensity
butyrate
succinate
C. clostridioforme
B. caecimuris
co-culture